PAPER

Diversified plasmonic metallic nanostructures with high aspect ratio based on templated electrochemical deposition

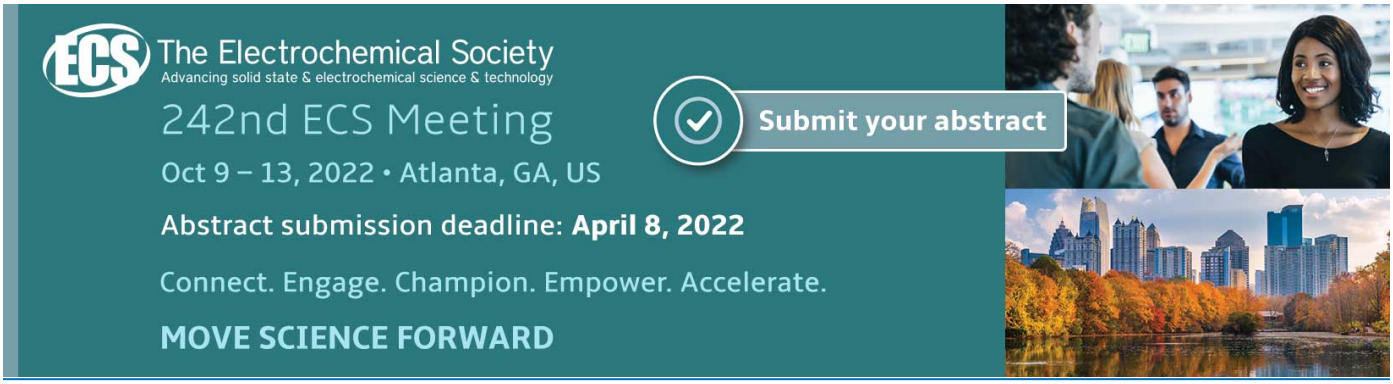

IOP Publishing Journal of Micromechanics and Microengineering
J. Micromech. Microeng. **32** (2022) 054002 (9pp) https://doi.org/10.1088/1361-6439/ac5b1b

Diversified plasmonic metallic nanostructures with high aspect ratio based on templated electrochemical deposition

Ruhao Pan[1,#], Qiulin Liu[1,#], Guodong Li[1], Yang Yang[1], Guangzhou Geng[1], Chensheng Li[1], Junxiang Yan[1], Zhongshan Zhang[1], Huaizhou Zhao[1], Changzhi Gu[1] and Junjie Li[1,2,*]

[1] Beijing National Laboratory for Condensed Matter Physics, Institute of Physics, Chinese Academy of Sciences, Beijing 100190, People's Republic of China
[2] Songshan Lake Materials Laboratory, Dongguan, Guangdong 523808, People's Republic of China

E-mail: jjli@iphy.ac.cn

Received 3 December 2021, revised 11 February 2022
Accepted for publication 7 March 2022
Published 18 March 2022

Abstract

Metallic high aspect ratio (HAR) nano-architectures provide new opportunities for a series of plasmonic devices due to their additional controllable degrees in height space compared to 2D patterns, but there is no efficient way that suitable for the rapid fabrication of large area HAR structures limited by the processing ability of traditional methods. Here in this work, we have developed a templated electrochemical deposition (ECD) method to fabricate various HAR metallic nano-structures for diversified plasmonic devices. The templated ECD method is based on the ECD filling of the nanopores that are fabricated by electron beam lithography. With this templated ECD method, numbers of HAR architectures including nanorods, nanofins and even mushroom-like structures, which have a line width as small as 100 nm and the aspect ratio up to 10:1, are established over a large scale. What is more, by simultaneously considering the designed layout and edge effect, sub 10 nm nanogap arrays are prepared, whose aspect ratio reaches 100:1 and the gap width reduces to 5 nm. Due to the extreme light confinement ability brought from Fabry–Perot resonance, the HAR nanogaps can be treated as a surface enhanced Raman scattering (SERS) substrate. Finite domain time difference simulation shows that fan-like 10 nm nanogap with a height of 700 nm has the largest light enhancement factor (EF). The configuration optimized nanogap is capable for the sensing of rhodamine 6G with a 10^{-9} M concentration. And the SERS EF of the nanogap is calculated to be 4×10^6, indicating the ultrasensitive molecular detection ability of the HAR nanogap. The templated ECD method not only brings a new chance for the construction of HAR metallic 3D structures, but also opens up a new horizon for the design of a series of plasmonic devices.

Keywords: nanogaps, high aspect ratio structure, surface enhanced Raman scattering, electrochemical deposition

(Some figures may appear in color only in the online journal)

* Author to whom any correspondence should be addressed.
# These authors contributed equally to this work.

1. Introduction

High aspect ratio (HAR) structures at micro/nano-scale have been widely concerned in the field of micro-electro-mechanical systems (MEMSs), electronic devices for their higher performance and richer functions compared to the planar patterns [1–4]. Especially, thanks to the controllable degrees along z-axis, HAR architectures can be efficiently applied in photonic components [5]. For instance, metamaterials and metasurfaces that consist of sub-wavelength units showing great ability in modulating the electromagnetic field [6]. And HAR structures in the metasurface help to realize the arbitrary controls of phase, amplitude of electromagnetic waves [7]. A series of metasurfaces based on HAR structures have been proposed with the abilities of light refraction or focus, structural color and even holographic imaging [8, 9]. Notably, the related devices are mostly based on dielectric structures. While metallic nano-structures, which possess the abilities of higher optical local enhancement factor (EF) and reflectivity compared to the dielectric components, can be potentially used in numbers of plasmonic devices, such as ultra-sensitive surface enhanced Raman scattering (SERS) substrates, reflection-type metasurfaces, and integrated optical micro/nano system etc [10–12]. HAR nanostructures potentially provides better ability of light confinement. However, there are still few reports that related to the HAR metallic structures due to the difficulties in the fabrications. In order to bring the HAR metallic structures into practical applications, a controllable, nano-scale, rapid fabrication method should be developed for large scale HAR nanostructures.

Unlike the dielectric HAR structures which can be easily built up by lithography and reactive ion etching (RIE) processes [13]. However, there are still problems in the construction of HAR metallic configurations by both chemical and physical methods. As for the chemical synthesis methods, the controllability of the configurations is hard to achieve for these methods due to their poor directionality, and the contamination of the materials is also inevitable. When it comes to physical methods including lithography, ion etching and physical vapor deposition (PVD), they show excellent ability in controlling the patterns, where planar structures with arbitrary shapes can be prepared for the applications in almost every field. Nevertheless, HAR metallic structures are unable to be obtained by these conventional physical methods, such as the physical etching methods cannot meet the requirement of etching the metal at a high speed and large selectivity, while considering the cost and the lift-off process, the PVD methods are incompatible for the achievement of thick material. In the past decade, numbers of 3D arts like 3D printing [14], focused ion beam (FIB) induced deposition [15], two-photon absorption [16], and tunable MEMS technologies [17] have been developed for the fabrication of 3D configurations, however, 3D printing method cannot realize the shapes in nanoscale, FIB induced deposition does not compatible to the large-area fabrication of HAR metallic structures, while two-photon absorption mostly used to build the polymer structures. And although MEMS technologies provide bended or folded HAR structures, the small feature sizes or thickness control of materials are hard to achieve. What is more, there are methods have been demonstrated based on coating the side walls of resist patterns for the take shape of HAR structures, however, these methods cannot be utilized for the metallic HAR configurations limited to the coated materials can only be dielectric [18–20]. Thus, there is no physical method that is suitable for the establishment of HAR metallic structures. Fortunately, electrochemical deposition (ECD), which is a process that the metal ions can be reduced and deposited on the cathode, gives a new possibility for the large area fabrication of thick metal [21, 22]. And there are HAR architectures with high quality Au have been demonstrated by combining the ECD method and lithography, which shows great potential in plasmonic applications [23–25]. But the extreme fabrication ability and application potentials for structures with varying cross-section and ultra-HAR have not effectively developed. Thus, there are still difficulties in the building up of HAR metallic structures.

Here in this work, we propose a templated ECD method for the fabrication of the HAR metallic structures, which possess the properties of large-area, nano-scale and excellent uniformity. The fabrication of the HAR structures includes the deposition of the conductive layer and the obtaining of the nanoscale templates by electron beam lithography (EBL). After that, ECD is introduced to fill the templates with metal. Because the metal can only be deposited on the conductive part of the substrate, thus there is no material that grows on the resist, meaning the materials waste and the lift-off process are avoided. Due to the resist patterns confines the metal growth along the and y direction during the ECD process, metallic architectures with line width as narrow as 100 nm and aspect ratio that exceeds 10:1 are obtained. Moreover, overgrowth effect is also considered in this work, once the metal height is larger than the resist thickness, mushroom-like structures can be fabricated due to the absence of horizontal growth restriction. Besides, by combining the layout design and the edge effect of EBL, nanogap with gap width down to 5 nm and aspect ratio up to 100:1 is taken shape over a large scale. Based on the strong light confinement effect of the nanogaps, we take the HAR nanogap array as a SERS substrate. A highest EF of 4×10^6 can be obtained for the nanogap with a height of 700 nm, which is compatible for the detection of rhodamine 6G (R6G) with a concentration of 10^{-9} M. The development of the templated ECD method provides a brand new method for the fabrication of HAR nanogaps, and further gives a fresh chance for the design of related photonics components and electronic devices.

2. Results and discussion

The fabrication of the HAR metallic structures starts from the cleaning of substrate (figure 1(a)), then a conductive layer is deposited on the substrate by PVD method as shown in figure 1(b). All kinds of metals can be used as the conductive layer, here in this work, Au is chosen for its superior conductivity. And polymethyl methacrylate (PMMA) with a thickness of 1 μm is spin coated onto the Au layer as the resist. EBL is applied to write the 2D patterns, as depicted in

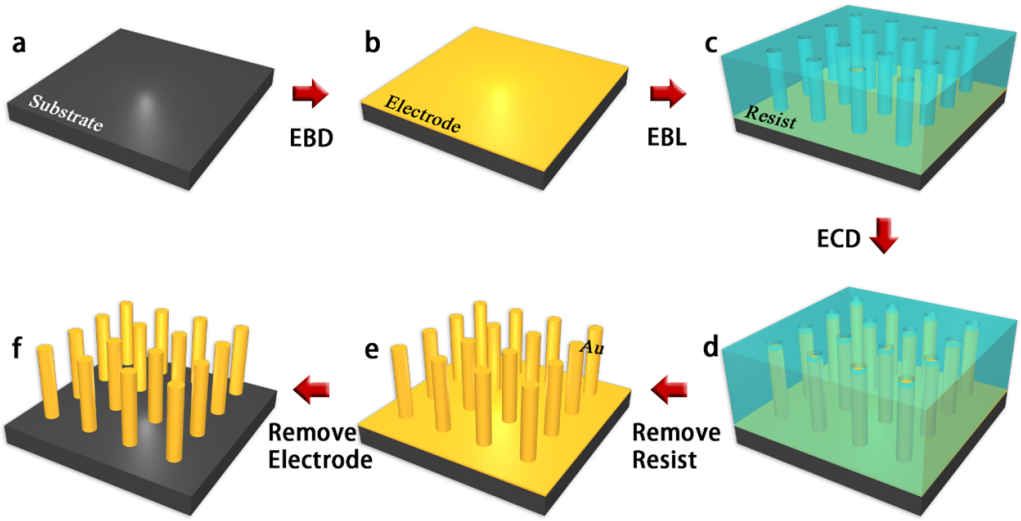

Figure 1. The schematics of the fabrication process for HAR structures. (a) Clean substrate; (b) the deposition of conductive layer; (c) the template obtained by spin coating and EBL; (d) the filling of Au by ECD; (e) HAR Au structures achieved by removing the resist; (f) etching of the conductive layer.

figure 1(c), the PMMA nanopores are taken shape after the development process. Notably, the EBL system has an accelerating voltage as high as 100 KV, which ensures the good steepness of the side walls of nanopores. After that, ECD is introduced to fill Au into the nanopores from the bottom of the nanopores up, take the substrate as the cathode of the ECD system and immersed it into the electrolyte, the Au+ ion can be reduced and deposited on the substrate under a certain voltage. Due to the Au can only be assembled on the conductive part of the cathode, the surface of the resist is immune from being covered, namely Au can be selectively grown in the nanopores (figure 1(d)). As figure 1(e) shows, the pattern transfer process was finally finished after remove the resist by RIE, and HAR metallic structures are obtained. What is more, the conductive layer can be further removed by ion milling (IM), and thus this method also suits for the building of independent Au structures (figure 1(f)). Here in this process, in order to avoid the void in the structures, the template is treated by O_2 plasma to remove the resist residual and enhance wettability. A 15 min stand is applied to the ECD system after the substrate is assembled, after that, a pipette is used to stir the electrolyte to minimize the bubbles in nanopores.

Following the process mentioned above, HAR structures can take shape, and their height controllability are analyzed in detail. Figure 2(a) depicts the voltage change with the deposition time increase. The current density in this process is fixed at 18.392 μA mm^{-2}, which can ensure the high quality of the Au structures. The roughness of the Au film is estimated to be 6.36 nm by atomic force microscope, meaning a smoother surface compared to the previous report [26], which is sufficient for the plasmonic applications. The inset in figure 2(a) gives the schematic of the ECD process, clearly showing the reduction and the accumulation effect of Au near the cathode. After removing the resist, figure 2(b) demonstrates the scanning electron microscopy (SEM) image of the Au configuration array, where the left picture was taken from the

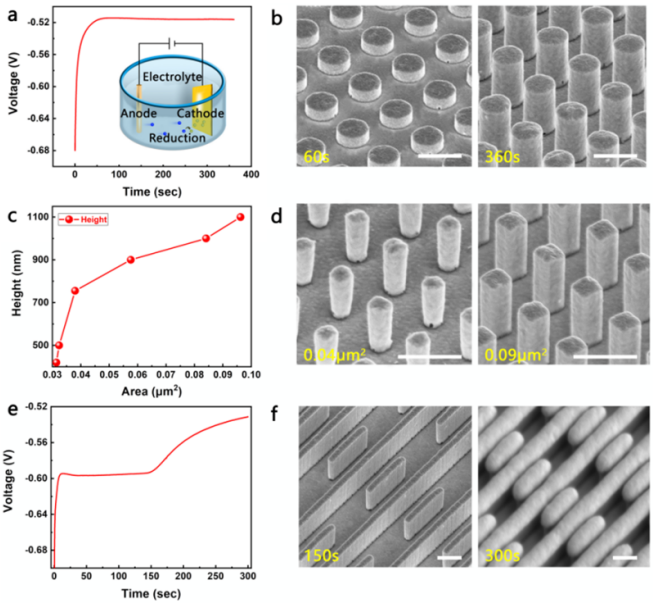

Figure 2. The controllability of the height and the configuration of the HAR structures. (a) The relationship between the voltage of ECD system and the deposition time; (b) scanning electron microscopy (SEM) images for the metallic pillar arrays under different ECD times; (c) the height of the HAR configurations as an equation with respect to the unit areas; (d) SEM image of metallic structures with different areas; (e) the curve of the deposition voltage versus the time; (f) SEM images for the not overgrown and overgrown nanostructures, respectively. Scale bars: 500 nm.

structure after 1 min ECD, the height of the nanorod is 100 nm. And after 6 min growth of Au, the right picture in figure 2(b) shows the nano-structures with HAR nanorods, whose height reaches 600 nm. Indicating the deposition speed of Au is 100 nm min^{-1}, both the height and the deposition speed can hardly be achieved by PVD method. The dependence between the lithography area of the unit cells and the height of the

HAR structures are statistics in figure 2(c), where the deposition time is 10 min. It can be clearly seen that with the area increasing from 0.03 to 0.1 μm^2, the deposition speed starts from ∼40 nm min^{-1} and rapidly increase to ∼80 nm min^{-1} when the unit cell area is 0.04 μm, and a largest speed of 110 nm min^{-1} can be finally achieved for the area of 0.1 μm^2. It is not difficult to find that the deposition speed relates to the area of the unit cell, the high growth speed can only be realized when the deposition area is large enough. This phenomenon maybe comes from the consumed Au+ ion in the nanopores by reduction should be replenished by the electrolyte away from the pores. However, the replenishment speed is limited by the area of nanopores, and lower speed happens to the smaller pore, and the concentration of the Au+ is shrunk for small pores, which in turn leads to a higher deposition speed with larger area. Figure 2(d) shows two arrays with unit cell of different areas, where the nanorods with larger area showing higher height compared to the smaller ones.

Basically, the templated ECD method is based on filling the nanopores that fabricated by EBL, which has a uniform section on the *x*–*y* plane. While the fabricated nanostructures' shape relies on the nanopores, resulting in the patterns on the bottom and the top of the HAR structures are the same. However, the structures with a cross section that changes with the height can be widely used in the field of ultra-sensitive sensing [27, 28] and optical resonators [29]. Fortunately, here in this work, the overgrowth effect of the templated ECD method can be controlled to build up nanostructures with cross section varying with height. As figure 2(e) shows, when the nanostructures are lower than the resist nanopores, the total deposition area is fixed, resulting in the deposition voltage are stabilized at ∼−0.6 V. Once the height of the nanostructures is larger than the thickness of resist, the overgrowth effect occurs, leading to the metal can spread along *x*–*y* plane due to the lack of resist limitation, and the increasing of the conductive area results in the decrease of the deposition voltage. During the overgrowth process, the cutting plane of the structures along *z*-axis can be modulated. As we can see from the left picture of figure 2(f), the SEM image which is collected from the HAR structures at the deposition voltage of 0.6 V, showing a uniform cross section pattern. While the right image shows an array of overgrown structures when the deposition voltage is 0.55 V, each unit cell proceeds a much larger top compared with the support part, indicating the cross section of the structures have changed. It should be noted that the SEM images in figure 2(f) are not the case in the same substrate, but from different samples obtained under the same deposition condition and different deposition time. The fabrication of the mushroom like structures further enriches the controllable degrees of freedom of the templated ECD method.

Thanks to the perfect structural controllability of both the height and the pattern of the templated ECD method, fascinating HAR configurations can be built up. Figure 3(a) depicts a large area array of nanorods, all the HAR nanofins in the array have a uniform configuration, showing the large area fabrication ability of the templated method. Figures 3(b) and (c) show arras of nanorods and nanofins with HAR, respectively, where the line widths of both structures are set to 100 nm,

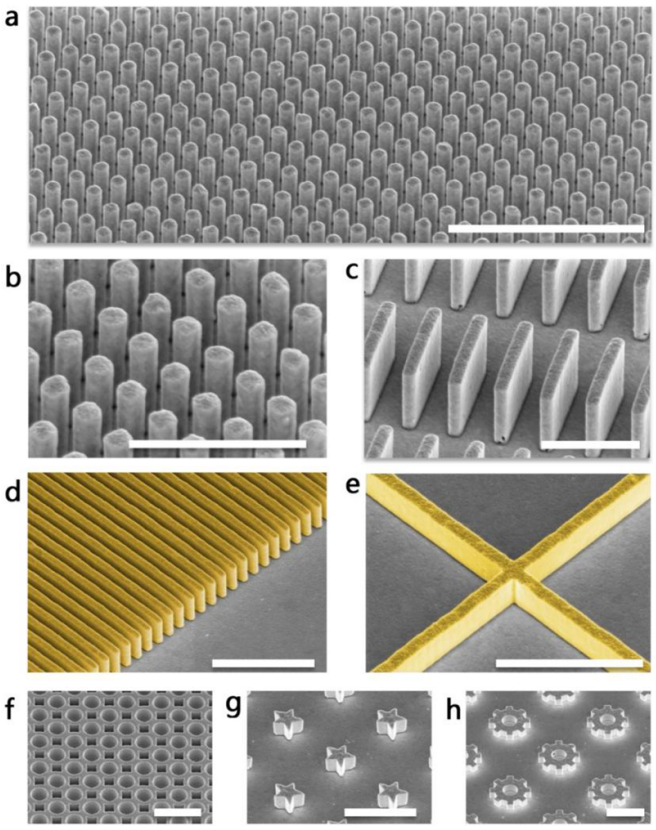

Figure 3. Diversified nanostructures fabricated by templated ECD method. (a) Large scale HAR nanostructures; (b) nanorods with aspect ratio up to 10:1; (c) HAR nanofins with an aspect ratio of 10:1; (d)–(h) the SEM images for HAR nanograting, cross-nanowalls, nanoholes, nanostars and microgears. Scale bars: (a) and (d)–(h) 2 μm; (b) and (c) 1 μm.

and the height of the configurations reaches more than 1 μm, meaning that their aspect ratio exceeds 10:1, which can hardly be achieved by the traditional method. Another point is the side walls of the configuration possess a smooth profile, which originates from the excellent filling ability of the ECD method, leading to the shape is exactly the profile of the resist template. Besides, HAR nanogratings and cross-nanowalls can also be obtained for series of plasmonic devices, as shown in figures 3(d) and (e). In the fields of electronics and photonics devices, the configurations of the nanostructures have a decisive effect on their performance, and the templated ECD method provides a new opportunity to realize the devices with arbitrary planar layout and height. More abundant and complex configurations have been prepared, such as the nanoholes, nanorings and microgears, which paves the way for the application of photonic, electronic and MEMS devices (figures 3(f)–(h)).

The arbitrary structural controllability of EBL to the planar pattern gives the templated ECD method a potential to the construction of the nanogaps, which is a nanoscale space between two metallic structures [30], with ultra-HAR. A major difficulty to obtaining nanogaps is how to control the ultra-small patterns. Here, the edge effect inevitably needs to be considered, which leads to the designed configuration is different from the output structure [31]. As demonstrated in figure 4(a),

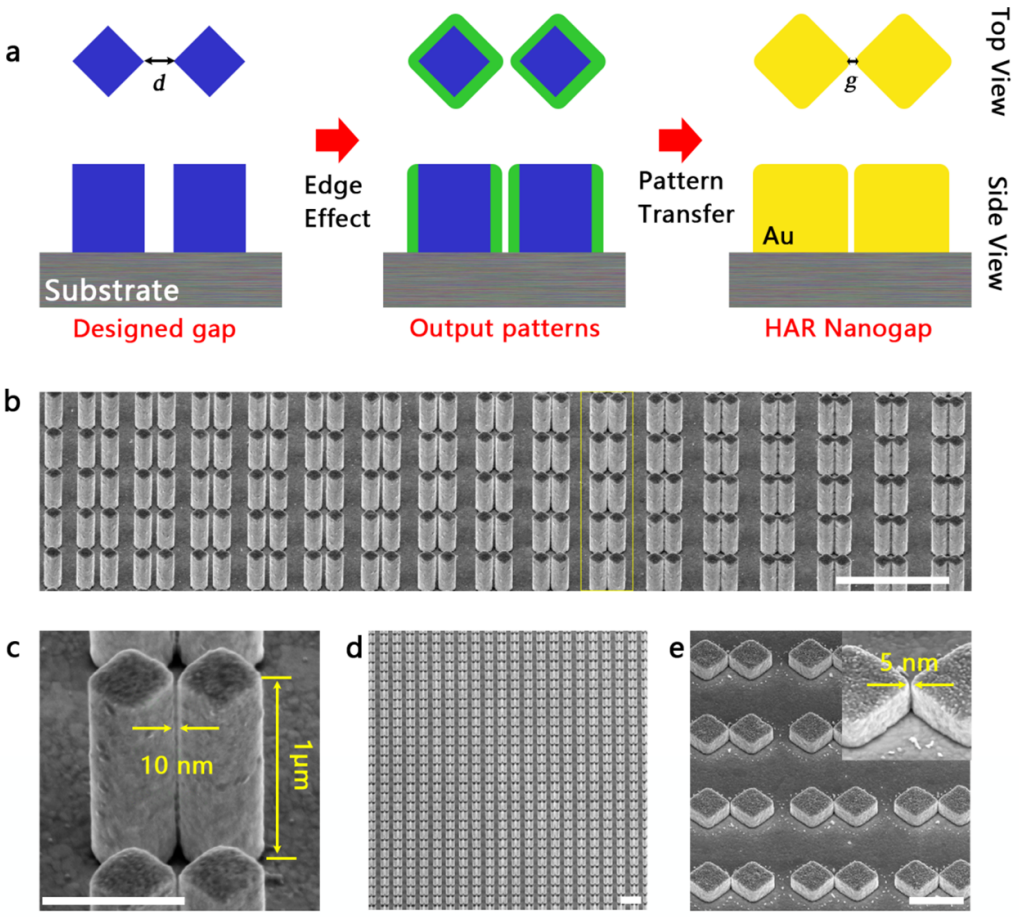

Figure 4. (a) Schematics of the pattern design, output nanopore, and the HAR nanogap; (b) SEM image of nanogaps with different widths; (c) an ultra-HAR nanogap with a width of 10 nm and height of 1 μm; (d) large area nanogaps; (e) an array of 5 nm gaps. Scale bars: (b) and (d) 2 μm; (c) and (e) 500 nm.

the target nanogap consists of two nanorods, where the distance between the nearest tips is labeled as d, and two blue rectangles in the left row are treated as the lithography layout. The edge effect appears in the EBL process, where the developed nanopores have a larger area than the designed ones due to the edge effect, as shown in the green edge of the middle row of figure 4(a). After the Au filling by ECD, the nanogaps are taken shape, it is obvious that the gap width g is smaller than the distance of the layout. By designing nanopatterns with different distances, the nanogaps are finally obtained by combining the layout design and edge effect, as shown in figure 4(b), from the left side to the right, the gap widths become smaller, and the red rectangle indicates a smallest gap width of sub 10 nm. By comparing the distance between the pattern and the width of the fabricated nanogap, it can be found that the edge effect introduced a 30 nm difference between the designed and output nanopores. Figure 4(c) shows a 10 nm gap with 1 μm height, whose aspect ratio reaches 100:1, which gives a large controllable degree of incident light along z-axis. Figure 4(d) depicts a 10 nm nanogap array, showing the excellent fabrication ability of the ECD method. In order to investigate the minimize gap width of the HAR nanogap. Nanogaps with a height of 150 nm are fabricated and a narrowest nanogap with 5 nm width can be found (figure 4(e)). The templated ECD method has proved to be effective in fabricating high resolution and HAR nanogap.

Based on the diversiform HAR structures that are developed by templated ECD method, a series of photonic and electronic devices can be realized. A SERS substrate based on the ultra-HAR nanogap array is fabricated to demonstrate its great potential in plasmonic devices. Figure 5(a) displays a nanogap array with the gap width fixed at 10 nm. The bottom electrode layer, which acts as a conductor during the ECD process, can introduces the charge transfer between the two nanorods of the nanogap. However, the charge transfer would give a negative influence to the light confinement effect. Thus, the IM is employed to the substrate to remove the bottom layer Au. As shown in figure 5(b), the Au can be efficiently removed, and a good uniformity can be observed between each nanogap. The inset shows a single nanogap after remove the bottom layer Au. Although the height of the nanogaps become lower, however the gap width is maintained at 10 nm, which origins from the good directionality of the ion etching, where the etching effect only happens to the z-axis rather than the x–y cross section. In order to verify the improvement of SERS intensity by removing the conductive Au layer, SERS spectra for R6G under a concentration of 10^{-4} M are collected from the substrates before and after the Au etching process,

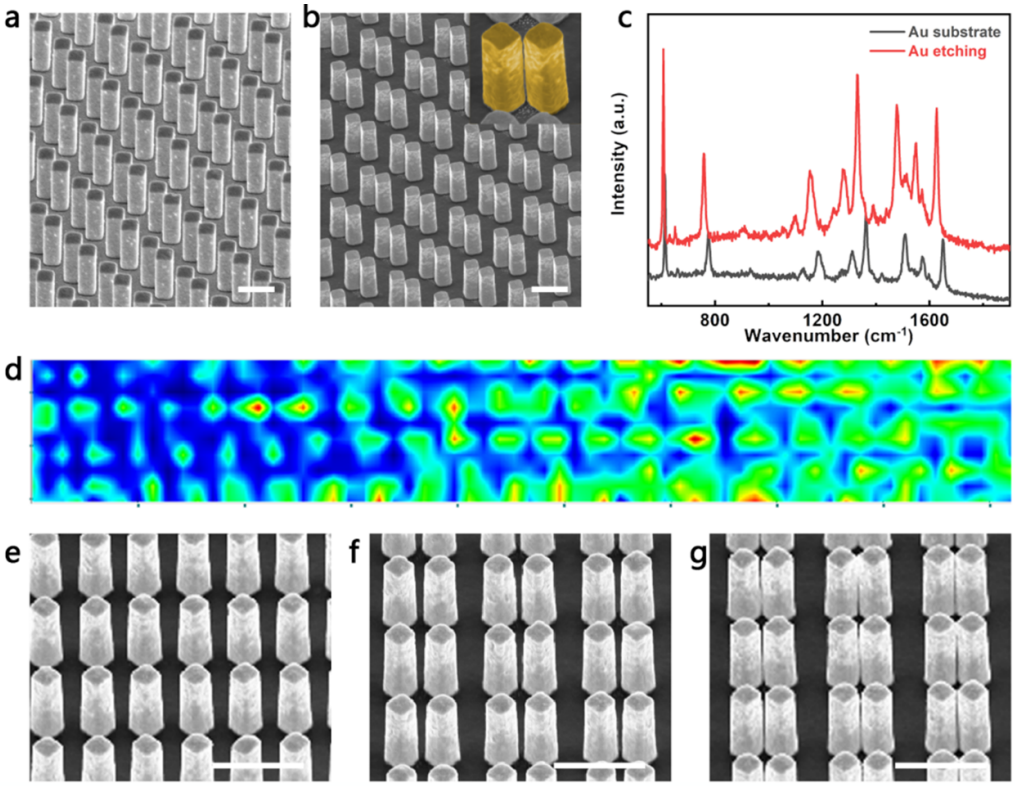

Figure 5. (a), (b) Metallic nanogaps with and without the bottom electrode, respectively, and their SERS spectra are shown in (c); (d) the SERS intensity distribution of the 613 cm^{-1} peak for the nanogap array with changing width; (e)–(g) SEM images of nanogaps with different widths. Scale bars: 1 μm.

respectively. As figure 5(c) shows, one can clearly see that the SERS intensities of characteristic peaks obtained from the nanogaps without Au bottom layer are much stronger than that before the Au etching. What is more, a SERS intensity mapping for 613 cm^{-1} peak is also collected from a nanogap array with changing gap width as shown in figure 5(d), as the gap width become smaller from the left side to the right side (figures 5(e)–(g)), the SERS signal increased, indicating the narrower gap provides higher SERS EF [32].

After the Raman enhancement property of the HAR nanogaps has been confirmed, a new configuration is designed to obtain higher SERS EF. As figure 6(a) shows, the nanorods of the nanogap are replaced by fan-like structures, which have been proved to have a much stronger light confinement compared to the rectangle pattern [33]. A schematic top view of the nanogap is shown at the bottom of figure 6(a), each fan-like pattern has an equilateral triangle, which has a vertex angle of $\theta = 105°$. And a half circle link to the bottom edge of the triangle, the distance between both center points of the half circle is $w = 0.4$ μm, and the radii of the half circles is $r = 0.3$ μm. Finite difference time domain (FDTD) method has been introduced to simulate the localized electric filed distribution of the nanogap, where the incident light is an x-polarized 532 nm Gaussian wave, all the boundaries are set to perfect matched layers to avoid reflection. Figure 6(b) depicts the top and side views of the local electric field distribution, a 'hot spot' can be observed in the nanogaps. Here, the nanogap can be seen as a nano-cavity, series of reflectance and interference happen in the nanogap, and the field intensity that is changed with the y-axis of the nanogap indicates the field enhancement effect origins from the Fabry–Perot resonance [34]. The field enhancement ability of the nanogap depends on the height of the nanogap, thus the light EF of nanogaps with different heights are further simulated and shown in figure 6(c), where two peaks can be observed for the gaps with 300 and 700 nm heights, respectively. In particular, the 10 nm gap with 700 nm height provides the highest light enhancement ability of $|E/E_0|^2 = 230$.

According to the simulated results, the nanogaps with periods of 2 and 1 μm along x- and y-axis, respectively, are fabricated by templated ECD method. Figure 6(d) displays a SEM image of nanogap array, indicating the nanogaps have a same configuration with the schematic. And the inset shows a single nanogap that is fabricated by templated ECD method, depicting a gap width of 10 nm and aspect ratio up to 70:1. Then the nanogap array is immersed into the R6G solution under concentrations of 10^{-4} and 10^{-9} M for 3 h in order to bond the R6G molecules on the surface of nanogaps. Then the Raman spectra are collected under the illumination of 532 nm laser with a power of 0.18 mW for 5 s. Figure 6(e) shows the SERS signal of 10^{-4} M R6G for Si, no nanogap structures and the nanogap substrate, where the Si substrate does not show obvious enhancement ability, while the spectrum collected from the no nanogap structures shows all the characteristic peaks for R6G. Notably, when it comes to the substrate based on nanogaps, the intensities of the characteristic

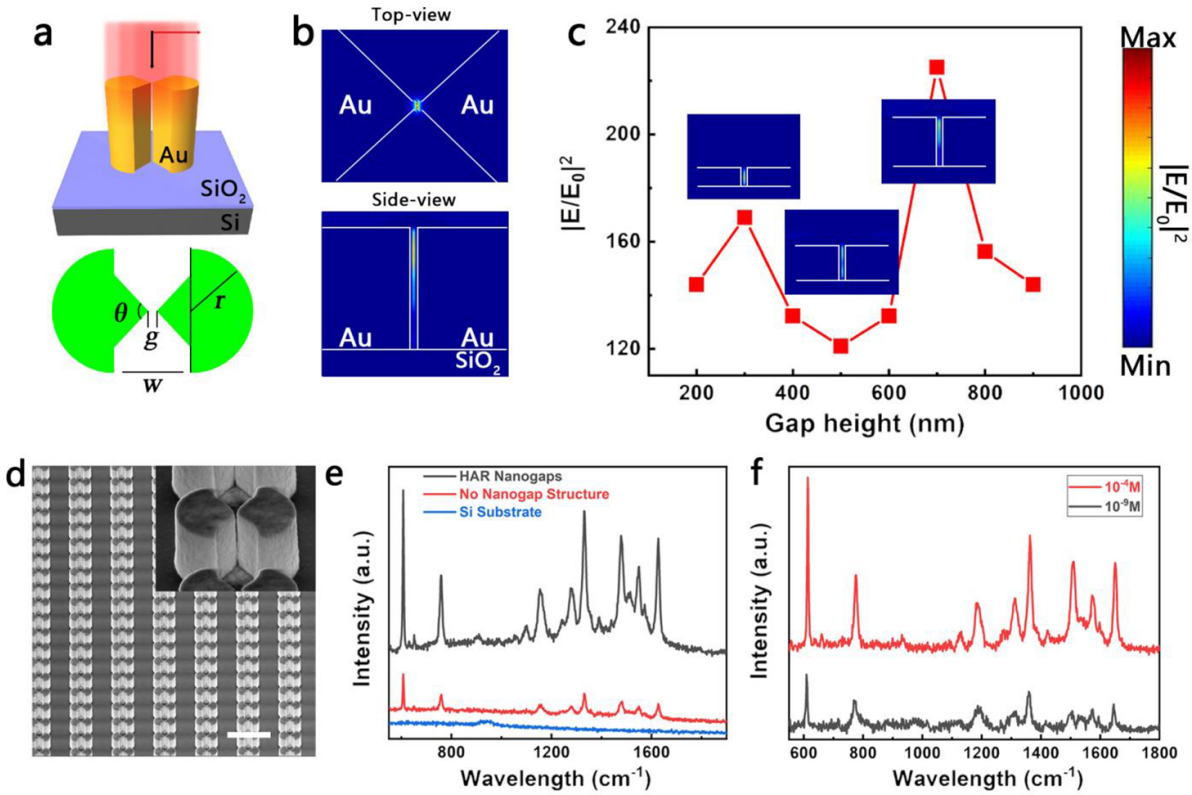

Figure 6. (a) Schematics of the configuration-optimized SERS substrate based on HAR nanogaps; (b) localized electric field distribution of the nanogap in the *x*–*y* and *x*–*z* planes; (c) the curve of light confinement versus the gap height; (d) fabricated SERS substrate, and the inset shows a unit cell in the substrate; (e) SERS spectra of R6G collected from Si, no nanogap structures and nanogap array, respectively; (f) SERS spectra of R6G under the concentrations of 10^{-4} and 10^{-9} M. Scale bar: 2 μm.

peaks are dramatically increased, indicating the nanogap plays the dominate part in enhancing the Raman signal. Figure 6(f) shows the large good enhancement ability of HAR nanogaps, apart from the signal intensity of 10^{-9} M R6G being smaller than that of 10^{-4} M, all the characteristic peaks can be distinctly distinguished. And the SERS EF are calculated by $EF = (N_{Bulk}/N_{SERS}) \times (I_{SERS}/I_{Bulk})$, where N_{Bulk} and I_{Bulk} refers to the excited molecular numbers and Raman intensity for R6G powder, while N_{SERS} and I_{SERS} are molecular numbers and SERS intensity of the R6G on the surface of the nanogap. Here the molecules on the nanogaps are treated as a monolayer. The EF of the nanogap is calculated to be 4×10^6, highlighting the ultra-sensitive SERS sensing ability of the HAR nanogaps. Notably, there are possibilities to further improve the SERS EF by optimizing the configuration of the substrate, such as inserting a gold layer blow the SiO_2 layer [35, 36].

3. Conclusions

In conclusion, we have demonstrated a templated ECD method for the fabrication of HAR metallic structures. Established structures have a minimum line-width down to 100 nm and aspect ratio reaches 10:1. Various HAR nanostructures including nanopores, nanorods, nanogratings have also been fabricated over a large scale, indicating the good uniformity and controllability of the templated ECD method. The overgrowth process has also been considered and modulated, mushroom-like architectures are effectively fabricated, which further improves the controllable degree of this method. Most importantly, by combining the layout design and the edge effect of EBL, HAR nanogaps can be obtained, whose width can be as narrow as 5 nm and the aspect ratio exceeds 100:1. Based on Fabry–Perot resonance of the HAR nanogaps, a SERS substrate is designed and realized with an EF of 4×10^6, which can be applied in the detection of R6G with a concentration of 10^{-9} M. The templated ECD method gives an efficiency approach for the rapid fabrication of large scale HAR metallic structures, which can be potentially used for the next generation of SERS substrates, metasurfaces and plasmon waveguides.

4. Methods

4.1. Fabrication process

The Si or SiO_2 substrates with 2 cm $\times$ 2 cm area were cleaned by a RIE (NGP80, Oxford) system, where the gas flow was O_2: 100 sccm to achieve a pressure of 100 mTorr, and the substrate was etched for 5 min under a power of 100 W. Then 50 nm Au was deposited on the substrate as a conductive layer. After that, 1 μm thick PMMA was spin-coated on the Au film for the

EBL exposure. The substrate was loaded in the EBL (JEOL, 6300FS) chamber, after EBL exposure, various patterns were developed in a mixture of methyl isobutyl ketone (MIBK) and isopropanol (IPA) with a ratio of 1:3. The substrate was further immersed into the Au electrolyte (NB technologies GmbH, NB Semiplate Au 100), take the Au film as the cathode while a platinized mesh as the anode, by fixing the current density as 18.392 μA mm^{-2}, the Au was deposited to fill the nanopores. After the Au filling, RIE is further used to remove the resist by the 100 W O_2 plasma etching under a pressure of 100 mTorr. And the HAR structures are finally obtained. Selectively, the conductive layer can be removed by IM under the Ar flow for 120 s, thus, individual metallic nano-structures based on Si or SiO_2 substrate are obtained.

4.2. Optical simulation method

The FDTD method was employed to simulate the electric field distribution of the nanogaps. The height of the nanogaps changed from 100 to 900 nm, while the substrate is a SiO_2 layer with a thickness of 1000 nm. The wavelength of the incidence light was set at 532 nm and propagated along the z-axis with the electric field polarized along the x-axis. Three monitors that are perpendicular to x, y, and z axes are set in the model, respectively, in order to capture the field distribution fully. All the simulated boundaries were perfectly matched layers to avoid reflections. Taking advantage of the model mentioned before, the field distribution of the HAR nanogaps on SiO_2 substrate is simulated.

4.3. SERS measurement

R6G powders were dissolved in deionized water to prepare solutions with different concentrations. The samples were functionalized with molecules by immersion in the solutions for 3 h. Then, the samples were taken out and washed by ethyl and deionized water (DI) to remove the unbound molecules, and then dried with a flow of nitrogen. The SERS measurements were carried out on a micro-Raman spectrometer (Horiba/Jobin Yvon HR 800) equipped with a 532 nm laser as the excitation source. The laser was focused on the sample surface using a 100× lens (N.A. = 0.9) with a 1 μm spot size. To protect the molecules from laser heating, the laser power was kept at 1.8 mW on the sample surface, and exposure times of 5 s are used to collect the SERS signal ranges from 550 to 1800 cm^{-1}. Each Raman spectrum was collected on a single gap. As for the calculation of SERS EF, a sample is immersed in 10^{-4} M concentration R6G for 3 h to bond a monolayer of R6G on the sample surface. And the depth of laser penetration for R6G powder is 2 μm. Using all the data mentioned before, the SERS EF can be calculated.

Data availability statement

All data that support the findings of this study are included within the article (and any supplementary files).

Acknowledgments

The authors acknowledge the financial support received from the National Natural Science Foundation of China (Grant Nos. 12074420, 11674387, 91323304, and 61905274), Beijing Municipal Science and Technology Commission, Administrative Commission of Zhongguancun Science Park (No. Z211100004821009), the Chinese Academy of Sciences through the Project for Young Scientists in Basic Research (YSBR-021), the Key Research Program of Frontier Sciences of Chinese Academy of Sciences (Grant No. QYZDJ-SSW-SLH042), the Key Deployment Project of Centre for Ocean Mega-Research of Science, Chinese Academy of Sciences (Grant No. COMS2020J03). and G Li acknowledges the funding support of Beijing Municipal Science and Technology Commission, Administrative Commission of Zhongguancun Science Park (No. 22D40121). This work is also supported by the Synergic Extreme Condition User Facility.

ORCID iDs

Ruhao Pan https://orcid.org/0000-0002-5573-2992
Yang Yang https://orcid.org/0000-0003-3785-9233
Guangzhou Geng https://orcid.org/0000-0003-3723-9632

References

[1] Chen B, Wang X, Gao B, Fang Z, Kang J, Liu L, Liu X, Lo G-Q and Kwong D-L 2014 Highly compact (4F^2) and well behaved nano-pillar transistor controlled resistive switching cell for neuromorphic system application *Sci. Rep.* **4** 6863
[2] Chen M-L *et al* 2020 A FinFET with one atomic layer channel *Nat. Commun.* **11** 1205
[3] Liu Z, Liu Z, Li J, Li W, Li J, Gu C and Li Z-Y 2016 3D conductive coupling for efficient generation of prominent Fano resonances in metamaterials *Sci. Rep.* **6** 27817
[4] Ma Y, Dong B and Lee C 2020 Progress of infrared guided-wave nanophotonic sensors and devices *Nano Converg.* **7** 12
[5] Guo P, Schaller R D, Ketterson J B and Chang R P H 2016 Ultrafast switching of tunable infrared plasmons in indium tin oxide nanorod arrays with large absolute amplitude *Nat. Photon.* **10** 267–73
[6] Chang Y, Wei J and Lee C 2020 Metamaterials—from fundamentals and MEMS tuning mechanisms to applications *Nanophotonics* **9** 3049–70
[7] Sroor H, Huang Y-W, Sephton B, Naidoo D, Vallés A, Ginis V, Qiu C-W, Ambrosio A, Capasso F and Forbes A 2020 High-purity orbital angular momentum states from a visible metasurface laser *Nat. Photon.* **14** 498–503
[8] Balthasar Mueller J P, Rubin N A, Devlin R C, Groever B and Capasso F 2017 Metasurface polarization optics: independent phase control of arbitrary orthogonal states of polarization *Phys. Rev. Lett.* **118** 113901
[9] Khorasaninejad M, Chen W T, Devlin R C, Oh J, Zhu A Y and Capasso F 2016 Metalenses at visible wavelengths: diffraction-limited focusing and subwavelength resolution imaging *Science* **352** 1190–4
[10] Dong B, Ma Y, Ren Z and Lee C 2020 Recent progress in nanoplasmonics-based integrated optical micro/nano-systems *J. Appl. Phys.* **53** 213001

[11] Hui X, Yang C, Li D, He X, Huang H, Zhou H, Chen M, Lee C and Mu X 2021 Infrared plasmonic biosensor with tetrahedral DNA nanostructure as carriers for label-free and ultrasensitive detection of miR-155 *Adv. Sci.* **8** e2100583
[12] Liu X, Liu W, Ren Z, Ma Y, Dong B, Zhou G and Lee C 2021 Progress of optomechanical micro/nano sensors: a review *Int. J. Optomechatron.* **15** 120–59
[13] Zhu Z *et al* 2014 M-shaped grating by nanoimprinting: a replicable, large-area, highly active plasmonic surface-enhanced Raman scattering substrate with nanogaps *Small* **10** 1603–11
[14] An B W, Kim K, Lee H, Kim S-Y, Shim Y, Lee D-Y, Song J Y and Park J-U 2015 High-resolution printing of 3D structures using an electrohydrodynamic inkjet with multiple functional inks *Adv. Mater.* **27** 4322–8
[15] Esposito M, Tasco V, Cuscunà M, Todisco F, Benedetti A, Tarantini I, Giorgi M D, Sanvitto D and Passaseo A 2014 Nanoscale 3D chiral plasmonic helices with circular dichroism at visible frequencies *ACS Photonics* **2** 105–14
[16] Liang Y, Lin H, Koshelev K, Zhang F, Yang Y, Wu J, Kivshar Y and Jia B 2021 Full-stokes polarization perfect absorption with diatomic metasurfaces *Nano Lett.* **21** 1090–5
[17] Ren Z, Chang Y, Ma Y, Shih K, Dong B and Lee C 2019 Leveraging of MEMS technologies for optical metamaterials applications *Adv. Opt. Mater.* **8** 1900653
[18] Desbiolles B X E, Bertsch A and Renaud P 2019 Ion beam etching redeposition for 3D multimaterial nanostructure manufacturing *Microsyst. Nanoeng.* **5** 11
[19] Laney S K, Li T, Michalska M, Ramirez F, Portnoi M, Oh J, Tiwari M K, Thayne I G, Parkin I P and Papakonstantinou I 2020 Spacer-defined intrinsic multiple patterning *ACS Nano* **14** 12091–100
[20] Geng G, Zhu W, Pan R, Zhang Z, Gu C and Li J 2021 Precise tailoring of multiple nanostructures based on atomic layer assembly via versatile soft-templates *Nano Today* **38** 101145
[21] Mandler D 2020 The future of electrochemical deposition: nanomaterial building blocks *J. Solid State Electrochem.* **24** 2133–5
[22] Li Z, Song Y, Fan C, Xu T and Zhang X 2021 Mini-pillar based multi-channel electrochemical platform for studying the multifactor silver electrodeposition *Electroanalysis* **33** 2401–5
[23] Päivänranta B, Merbold H, Giannini R, Büchi L, Gorelick S, David C, Löffler J F, Feurer T and Ekinci Y 2011 High aspect ratio plasmonic nanostructures for sensing applications *ACS Nano* **5** 6374–82
[24] Mueller A D, Tobing L Y M and Zhang D H 2019 Reliable fabrication of high aspect ratio plasmonic nanostructures based on seedless pulsed electrodeposition *Adv. Mater. Technol.* **4** 1800364
[25] Gorelick S, Guzenko V A, Vila-Comamala J and David C 2010 Direct e-beam writing of dense and high aspect ratio nanostructures in thick layers of PMMA for electroplating *Nanotechnology* **21** 295303
[26] Kurashima Y, Maeda A and Takagi H 2014 Replication of atomically smooth surface shape onto electroplated Au patterns by lift-off process and room-temperature Au–Au bonding in atmospheric air *Microelectron. Eng.* **129** 1–4
[27] Zhu C, Meng G, Zheng P, Huang Q, Li Z, Hu X, Wang X, Huang Z, Li F and Wu N 2016 A hierarchically ordered array of silver-nanorod bundles for surface-enhanced Raman scattering detection of phenolic pollutants *Adv. Mater.* **28** 4871–6
[28] Hatab N A, Hsueh C H, Gaddis A L, Retterer S T, Li J H, Eres G, Zhang Z and Gu B 2010 Free-standing optical gold bowtie nanoantenna with variable gap size for enhanced Raman spectroscopy *Nano Lett.* **10** 4952–5
[29] Lee S A, Kang H S, Park J K and Lee S 2014 Vertically oriented, three-dimensionally tapered deep-subwavelength metallic nanohole arrays developed by photofluidization lithography *Adv. Mater.* **26** 7521–8
[30] Zhou Z, Zhao Z, Yu Y, Ai B, Mohwald H, Chiechi R C, Yang J K and Zhang G 2016 From 1D to 3D: tunable sub-10 nm gaps in large area devices *Adv. Mater.* **28** 2956–63
[31] Kim M-K, Sim H, Yoon S J, Gong S-H, Ahn C W, Cho Y-H and Lee Y-H 2015 Squeezing photons into a point-like space *Nano Lett.* **15** 4102–7
[32] Zhu W and Crozier K B 2014 Quantum mechanical limit to plasmonic enhancement as observed by surface-enhanced Raman scattering *Nat. Commun.* **5** 5228
[33] Brown L V, Yang X, Zhao K, Zheng B Y, Nordlander P and Halas N J 2015 Fan-shaped gold nanoantennas above reflective substrates for surface-enhanced infrared absorption (SEIRA) *Nano Lett.* **15** 1272–80
[34] Pan R, Yang Y, Wang Y, Li S, Liu Z, Su Y, Quan B, Li Y, Gu C and Li J 2018 Nanocracking and metallization doubly defined large-scale 3D plasmonic sub-10 nm-gap arrays as extremely sensitive SERS substrates *Nanoscale* **10** 3171–80
[35] Chanda D, Shigeta K, Truong T, Lui E, Mihi A, Schulmerich M, Braun P V, Bhargava R and Rogers J A 2011 Coupling of plasmonic and optical cavity modes in quasi-three-dimensional plasmonic crystals *Nat. Commun.* **2** 479
[36] Xiang Q, Zhu X, Chen Y and Duan H 2016 Surface enhanced Raman scattering of gold nanoparticles supported on copper foil with graphene as a nanometer gap *Nanotechnology* **27** 075201